Smart Structures and Systems, *Vol. 18, No. 4 (2016) 819-837*
DOI: http://dx.doi.org/10.12989/sss.2016.18.4.819

Reproduction of vibration patterns of elastic structures by block-wise modal expansion method (BMEM)

B.K. Jung[1], J.R. Cho[*2] and W.B. Jeong[1]

[1]*School of Mechanical Engineering, Pusan National University, Busan 609-735, Korea*
[2]*Department of Naval Architecture and Ocean Engineering, Hongik University, Sejong 339-710, Korea*

(Received June 17, 2016, Revised July 30, 2016, Accepted August 5, 2016)

Abstract. The quality of vibration pattern reproduction of elastic structures by the modal expansion method is influenced by the modal expansion method and the sensor placement as well as the accuracy of measured natural modes and the total number of vibration sensors. In this context, this paper presents an improved numerical method for reproducing the vibration patterns by introducing a block-wise modal expansion method (BMEM), together with the genetic algorithm (GA). For a given number of vibration sensors, the sensor positions are determined by an evolutionary optimization using GA and the modal assurance criterion (MAC). Meanwhile, for the proposed block-wise modal expansion, a whole frequency range of interest is divided into several overlapped frequency blocks and the vibration field reproduction is made block by block with different natural modes and different modal participation factors. A hollow cylindrical tank is taken to illustrate the proposed improved modal expansion method. Through the numerical experiments, the proposed method is compared with several conventional methods to justify that the proposed method provides the improved results.

Keywords: vibration pattern reproduction; block-wise modal expansion method (BMEM); sensor placement optimization; modal assurance criterion (MAC); genetic algorithm (GA)

1. Introduction

The structural vibration response of an elastic structure subject to the external excitation is expressed by a linear combination of the natural modes (i.e., the mode superposition), where the contribution of each natural mode is influenced by the frequency response characteristic of external excitation. Thus, the acquisition of natural modes becomes a first and most important step for the vibration analysis of structural dynamic systems. In fact, the structural modal identification plays an important role in the structural model updating, vibration pattern visualization, structural health monitoring and the optimum control of structural systems (Jiménez and De Frutos 2005, Yi *et al*. 2012). The natural frequencies and natural modes, called the modal parameters for the structural modal identification, could be obtained either by the vibration test or by the finite element modal analysis (Friswell and Mottershead 1995). But, since a real structure under external excitation exhibits a quite distinct vibration behavior point by point and direction by direction, the

∗Corresponding author, Associate Professor, E-mail: jrcho@hongik.ac.kr

http://www.techno-press.org/?journal=sss&subpage=8 ISSN: 1738-1584 (Print), 1738-1991 (Online)

reliability of the modal identification is substantially influenced by the quality of measured modal parameters.

In reality, the acquisition of modal parameters is always incomplete owing to the limited number of exciters and sensors, the measurement error in vibration test and the limitation of finite element models (McConnell 1995, Papadimitriou 2004). Here, the term *incomplete* means that not only the number of measured natural modes is finite but the error is included in the measured data. In this context, a sufficient number of modal parameters are recommended to be taken into the mode superposition. There is no doubt that the superposition of inaccurate natural models provides the point-wise dynamic responses and the overall vibration patterns which are far from the exact ones. In particular, it becomes more critical for the modal expansion when the quantities associated with the extended natural modes are derived based on the measured modal parameters (Allaei and Soedel 1986). In case of vibration test, the use of limited number of exciters and sensors naturally leads to the necessity of optimum placement of exciters and sensors (Hiramoto *et al*. 2000, Stephan 2012), in order to acquire the limited number of modal parameters as accurate as possible.

Traditionally, the placement of exciters and sensors was made by one's own decision making appealing to his intuition or/and empirical know-how, so that this kind of trial-and-error approach may not guarantee the sufficiently informative modal parameters. Regarding the development of sensor placement methodology, Poston and Tolson (1992) introduced an effective independence (EI) method in which a number of candidate sensor positions are eliminated or added by the determinant of a Fisher information matrix (FIM). Papadimitriou *et al.* (2004) used the information entropy norm (IEN) to suppress the uncertainty in modal parameter testing, in which the optimum sensor configuration is sought by minimizing the information entropy norm. Hiramoto *et al.* (2000) applied the explicit solution of algebraic Riccati equation to the optimal sensor/actuator placement for active vibration control. As an effective alternative approach to the above-mentioned heuristic algorithms, the use of genetic algorithm (GA) has been also proposed by subsequent investigators (Han and Lee 1999, Jung *et al*. 2015). Yi *et al.* (2011) proposed a hybrid sensor placement optimization method for structural health monitoring based on multiple optimization strategies by utilizing the QR factorization, the sequential sensor placement algorithm and the generalized genetic algorithm (GGA). More recently, they introduced a multiaxial sensor placement optimization for structural health monitoring by making use of the triaxial modal assurance criterion and a distributed wolf algorithm (2013, 2016).

The visualization of vibration pattern of elastic structure has become an important subject, in the structural vibration community, to which the modal parameters can be usefully applied (Larson *et al*. 1994, Sas *et al*. 1995, Garden and Fanning 2004). The overall vibration pattern helps one to easily figure out the vibration characteristic of a structural system, and furthermore the structural state could be diagnosed by monitoring the vibration patterns. As illustrated in Fig. 1, the vibration pattern of a structure at a specific frequency could be reproduced either by using the virtual instrument (Jiménez and De Frutos 2005) or by utilizing the modal expansion method (MEM) (Bernard and Bronowicki 1994, Lin and Parker 1999, Chen 2010). In case of the modal expansion method, the overall vibration patterns are reproduced with the limited number of the natural modes and the modal participation factors. Differing from the mode superposition method (Cho and Lee 2001) in which the vibration response is predicted using the known natural modes, the modal expansion method conversely predicts the modal participation factors using the measured vibration response data. Thus, the quality of vibration pattern reproduction is influenced by the modal expansion technique as well as the sensor positions when the total number of modal parameters is limited.

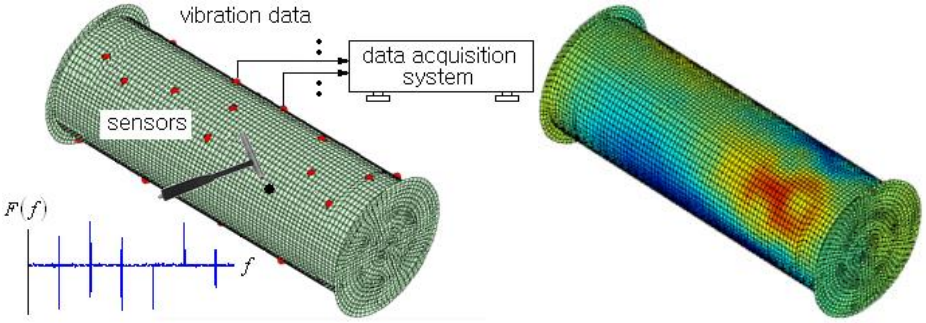

Fig. 1 Vibration pattern visualization of a hollow cylindrical structure at a specific frequency

In order for the numerical reproduction of vibration patterns of elastic structures, the basic and residual modal expansion methods are widely employed. However, it is known that the quality of reproduced vibration pattern by the basic MEM is definitely influenced by the number of selected natural modes. Moreover, the selection method of natural modes as well as the sensor positions does also influence the accuracy of vibration pattern reproduction. The numerical inaccuracy stemming from the limited number of natural modes could be resolved by the residual MEM to some extent, in which the effect of discarded high-order natural modes is accounted through the numerical manipulation. However, the improvement could be possible only when the total number of measured vibration data is not the same with the total number of selected natural modes. This condition will be addressed in details later in Section 3.2.

As an extension of our previous work on the sensor placement optimization (Jung *et al*. 2015), this paper intends to introduce an improved modal expansion method, called the block-wise modal expansion (BMEM), for the accurate reproduction of vibration patterns of elastic structures with the help of genetic algorithm (GA). A whole frequency range of interest is divided into several overlapped frequency blocks and the vibration field reproduction is made block by block. The number of natural modes selected for the vibration pattern reproduction is kept the same for all the frequency blocks, but the total numbers of the natural modes and the modal participation factors are taken differently for different frequency blocks. Meanwhile, for the given number of vibration sensors, the sensor positions for measuring the vibration responses that are required to determine the modal participation factors are determined by the GA-based sensor placement optimization. Through the numerical experiments with a hollow cylindrical structure, the reproduced vibration patterns as well as the frequency responses are compared with the basic MEM, the residual MEM, and two commercial codes, MSC/Nastran and ABAQUS.

2. Sensor placement and conventional modal expansion methods

In this section, we briefly address the sensor placement and modal assurance criterion (MAC) that are essential for the modal identification. As well, we review the conventional basic modal expansion method (MEM) and its refined form, called the residual modal expansion method (RMEM), in which some of discarded high-order natural modes are considered.

2.1 Sensor placement

For the sake of explanation purpose, let us consider the positioning of N sensors to identify the natural modes of a rectangular plate shown in Fig. 2(a). We assume that the plate domain is discretized into a finite element mesh having m degrees of freedom (DOFs), and only the lowest $n(n<m)$ natural modes $[\boldsymbol{\Phi}]_{m\times n}=\{\boldsymbol{\Phi}_1,\boldsymbol{\Phi}_2,\cdots,\boldsymbol{\Phi}_n\}$ are selected for the vibration pattern reproduction. Here, $\boldsymbol{\Phi}_I$ are defined by $\{\phi_I^1,\phi_I^2,\cdots,\phi_I^m\}^T$ with the total of m components. Furthermore, the reduced numerical natural modes $[\boldsymbol{\Phi}^r]_{N\times n}=\{\boldsymbol{\Phi}_1^r,\boldsymbol{\Phi}_2^r,\cdots,\boldsymbol{\Phi}_n^r\}$ identified by $N(N<n)$ sensors are assumed to be constructed from the selected modes $[\boldsymbol{\Phi}]_{m\times n}$ among the original natural modes $[\boldsymbol{\Phi}^{org}]$ obtained by the FE modal analysis. Then, each reduced numerical natural mode $\boldsymbol{\Phi}_I^r$ having the reduced number of components is defined by

$$\boldsymbol{\Phi}_I^r=\{\phi_I^1,\phi_I^2,\cdots,\phi_I^N\}^T,\quad I=1,2,\cdots,n \tag{1}$$

in which ϕ_I^i denote the components in $\boldsymbol{\Phi}_I$ which correspond to the finite element nodes having the vibration sensors.

Meanwhile, the correlation between two natural modes is usually evaluated by the modal assurance criterion (MAC) defined by (Allemang and Brown 1982)

$$MAC_{IJ}=MAC(\boldsymbol{\Phi}_I^T\boldsymbol{\Phi}_J)=\frac{\left|\boldsymbol{\Phi}_I^T\boldsymbol{\Phi}_J\right|^2}{(\boldsymbol{\Phi}_I^T\boldsymbol{\Phi}_I)(\boldsymbol{\Phi}_J^T\boldsymbol{\Phi}_J)} \tag{2}$$

where $\boldsymbol{\Phi}_I$ and $\boldsymbol{\Phi}_J$ denote two natural mode vectors of interest. The possible range of the MACs is from zero to unity such that two vectors $\boldsymbol{\Phi}_I$ and $\boldsymbol{\Phi}_J$ are the same when it is unity while both are in no correlation when it is zero. The MAC can be used to evaluate the correlation between the reduced numerical modes when $\boldsymbol{\Phi}_I$ and $\boldsymbol{\Phi}_J$ in Eq. (2) are replaced with $\boldsymbol{\Phi}_I^r$ and $\boldsymbol{\Phi}_J^r$, furthermore it can be also used to correlate the reduced numerical modes $\boldsymbol{\Phi}_J^r$ with the experimentally-measured modes $\hat{\boldsymbol{\Phi}}_I$. In the latter case, the definition given by $\mathrm{MAC}_{IJ}=max_J(\mathrm{MAC}_{IJ})$ seeks a numerical mode which is best fit to the *I*–th experimental mode (Brehm 2010).

Fig. 2(b) illustrates MAC of the reduced numerical modes $\boldsymbol{\Phi}_I^r$ corresponding to the 10 sensor positions on the rectangular plate shown in Fig. 2(a). The orthogonality between the reduced numerical modes increases as the off-diagonal values decrease to zero while the diagonal terms approach to unity. This example demonstrates the importance of sensor placement when the natural modes of elastic structure are extracted by experiment using a limited number of vibration sensors. In other words, the modal identification of elastic structure by experiment becomes more accurate as the sensor placement produces the MAC closer to the above-mentioned ideal one. In this context, the sensor placement optimization is desired to be made by minimizing the objective function $F(\mathbf{X})$ defined by

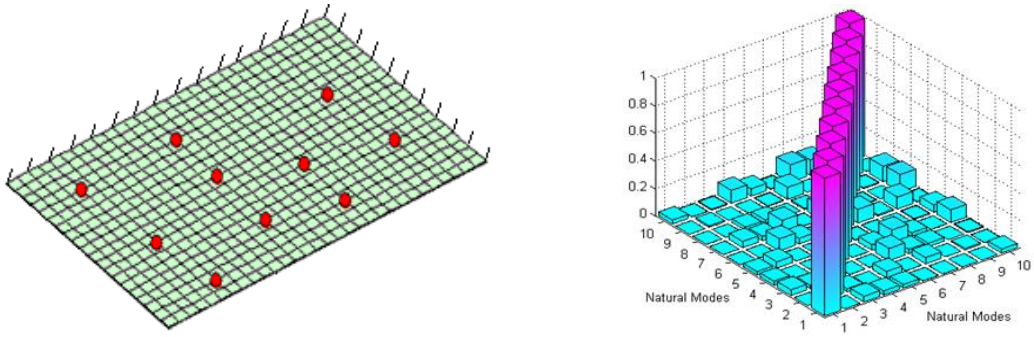

(a) (b)

Fig. 2 A vibrating plate: (a) sensor placement and (b) modal assurance criterion (MAC)

$$F(\mathbf{X}) = \sum_{I,J=1, I<J}^{N} MAC_{IJ}(\mathbf{X}) \tag{3}$$

Here, $\mathbf{X}$ denotes the $(2N \times 1)$ design variable vector $\left\{\mathbf{x}_1^s, \mathbf{x}_2^s, \cdots, \mathbf{x}_N^s\right\}^T$ containing the position vectors $\mathbf{x_i} = (x_i, y_i)^T$ of N vibration sensors.

In the current study, the n reduced numerical natural modes $\mathbf{\Phi}_I^r$ are constructed from the n lowest natural modes $\mathbf{\Phi}_I$. This implies that those would be lowest natural modes satisfying the orthogonality if their MAC becomes diagonal. Because the vibration pattern is to be expanded with the n reduced numerical natural modes $\mathbf{\Phi}_I^r$, the mode expansion would lead to the best result when the MAC becomes diagonal. In this context, the sum of the off-diagonal terms could be an indication (Yi *et al.* 2011) not only for the optimum sensor placement but also for the best mode expansion.

2.2 Conventional modal expansion methods (MEMs)

Basically, the numerical approximation of a damped structural vibration problem using a $m-$ DOF finite element mesh ends up with the system of linear matrix equations given by

$$[\mathbf{M}]\ddot{\bar{\mathbf{u}}} + [\mathbf{C}]\dot{\bar{\mathbf{u}}} + [\mathbf{K}]\bar{\mathbf{u}} = \mathbf{F} \tag{4}$$

with $\bar{\mathbf{u}}$ being the nodal displacement vector. Substituting the mode superposition $\bar{\mathbf{u}}(\mathbf{x}; t) = [\mathbf{\Phi}(\mathbf{x})]\mathbf{q}(t)$ using the selected natural modes into Eq. (4) and multiplying the $(n \times n)$ matrix $[\mathbf{\Phi}]^{\mathrm{T}}$ of selected natural modes leads to

$$[\mathbf{\Phi}]^{\mathrm{T}}[\mathbf{M}][\mathbf{\Phi}]\ddot{\mathbf{q}} + [\mathbf{\Phi}]^{\mathrm{T}}[\mathbf{C}][\mathbf{\Phi}]\dot{\mathbf{q}} + [\mathbf{\Phi}]^{\mathrm{T}}[\mathbf{K}][\mathbf{\Phi}]\mathbf{q} = [\mathbf{\Phi}]^{\mathrm{T}}\mathbf{F} \tag{5}$$

where $\mathbf{q}$ is the $(n\times 1)$ vector of modal participation factors. From the orthonormality between the natural modes, one can obtain the relation between the modal participation factors q_I and the normalized forces $Q_I = \mathbf{\Phi}_I^T \mathbf{F}$ for the harmonic response

$$\left[\left(\omega_I^2 - \omega^2\right) + 2\zeta\omega_I\omega\right] q_I = Q_I, \quad I = 1, 2, \cdots, n \tag{6}$$

In the mode superposition method, the coefficients q_I are determined using Eq. (6) for the known Q_I and the damping ratio ς, and then the structural vibration response $\bar{\mathbf{u}}(\mathbf{x};t)$ is to be obtained.

However, in the basic MEM, the vibration pattern is reproduced in terms of the reduced selected modes $\left[\mathbf{\Phi}^r\right]_{N\times n} = \left\{\mathbf{\Phi}_1^r, \mathbf{\Phi}_2^r, \cdots, \mathbf{\Phi}_n^r\right\}$ and $\mathbf{q}_{n\times 1}$ which are determined from the measured nodal response $\bar{\mathbf{u}}^m(\mathbf{x};t)$ at N sensor positions. With the selected natural modes and the measured nodal responses, the relation given by $\bar{\mathbf{u}}_{N\times 1}^m = \left[\mathbf{\Phi}^r\right]_{N\times n}\mathbf{q}_{n\times 1}$ leads to

$$\mathbf{q}_{n\times 1} = \left[\mathbf{\Phi}^r\right]_{n\times N}^{\uparrow} \bar{\mathbf{u}}_{N\times 1} \tag{7}$$

to determine the modal participation factors $\mathbf{q}$, where $\left[\mathbf{\Phi}^r\right]^{\uparrow} = \left(\left[\mathbf{\Phi}^r\right]^T\left[\mathbf{\Phi}^r\right]\right)^{-1}\left[\mathbf{\Phi}^r\right]^T$ denotes the left generalized inverse matrix of $\left[\mathbf{\Phi}^r\right]$ (Li *et al*. 2013). Then, the vibration field $\mathbf{u}(\mathbf{x};t)$ can be reproduced in terms of the nodal displacements calculated by

$$\mathbf{u}_{p\times 1} = \left[\mathbf{\Phi}^r\right]_{p\times n}\mathbf{q}_{n\times 1}, \quad N \le p \le n \tag{8}$$

using the modal participation factors and the natural modes.

On the other hand, the RMEM accounts for the contribution by some of the discarded higher-order natural modes $[\mathbf{\Psi}] = \left[\mathbf{\Phi}_{n+1}, \mathbf{\Phi}_{n+2}, \cdots, \mathbf{\Phi}_m\right]$, where the total number of $(m-n)$ higher-order modes will be denoted by $\tilde{n}$ in this paper. Meanwhile, the whole nodal displacement $\bar{\mathbf{u}}_{n\times 1}(\mathbf{x};t)$ is decomposed into the measured part $\bar{\mathbf{u}}_{N\times 1}^m(\mathbf{x};t)$ by the vibration sensors and the unmeasured part $\bar{\mathbf{u}}_{\tilde{N}\times 1}^u(\mathbf{x};t)$ such that

$$\bar{\mathbf{u}}_{n\times 1}(\mathbf{x};t) = \bar{\mathbf{u}}_{N\times 1}^m(\mathbf{x};t) + \bar{\mathbf{u}}_{\tilde{N}\times 1}^u(\mathbf{x};t) \tag{9}$$

with $\tilde{N}$ being $n-N$. The two parts are superposed in terms of the reduced natural modes and the modal participation factors

$$\begin{Bmatrix}\bar{\mathbf{u}}^m \\ \bar{\mathbf{u}}^{\mathbf{u}}\end{Bmatrix} = \begin{bmatrix}\left[\mathbf{\Phi}^{r,m}\right] & \left[\mathbf{\Psi}^{r,m}\right] \\ \left[\mathbf{\Phi}^{r,u}\right] & \left[\mathbf{\Psi}^{r,u}\right]\end{bmatrix}\begin{Bmatrix}\mathbf{q} \\ \tilde{\mathbf{q}}\end{Bmatrix} \tag{10}$$

Here, the superscripts (r,m) and (r,u) stand for the reduced selected and unselected modes at N measured and $\tilde{N}$ unmeasured positions, respectively. And, $\mathbf{q}_{n\times 1}$ and $\tilde{\mathbf{q}}_{\tilde{n}\times 1}$ denote the modal participation factors of the selected and unselected natural modes, respectively.

The modal participation factors $\mathbf{q}_{n\times 1}$ can be determined by the basic MEM as given in Eq. (7).

Let us split Eq. (10) into two matrix equations as follows

$$\bar{\mathbf{u}}^{\mathbf{m}}_{\mathbf{N}\times 1} = \left[\boldsymbol{\Phi}^{r,m}\right]_{N\times n}\mathbf{q}_{n\times 1} + \left[\boldsymbol{\Psi}^{r,m}\right]_{N\times \tilde{n}}\tilde{\mathbf{q}}_{\tilde{n}\times 1} \tag{11}$$

$$\bar{\mathbf{u}}^{u}_{\tilde{\mathbf{N}}\times 1} = \left[\boldsymbol{\Phi}^{r,u}\right]_{\tilde{N}\times n}\mathbf{q}_{n\times 1} + \left[\boldsymbol{\Psi}^{r,u}\right]_{\tilde{N}\times \tilde{n}}\tilde{\mathbf{q}}_{\tilde{n}\times 1} \tag{12}$$

in order to derive the relation between $\mathbf{q}_{n\times 1}$ and $\tilde{\mathbf{q}}_{\tilde{n}\times 1}$. In a similar manner to $\left[\boldsymbol{\Phi}^{r,m}\right]$, three reduced mode matrices $\left[\boldsymbol{\Phi}^{r,u}\right]$, $\left[\boldsymbol{\Psi}^{r,m}\right]$ and $\left[\boldsymbol{\Psi}^{r,u}\right]$ can be constructed from Eq. (1) using the selected and unselected natural modes. Pre-multiplying $\left[\boldsymbol{\Psi}^{r,m}\right]$ to Eq. (11) and rearranging the resulting equation leads to

$$\left[\boldsymbol{\Psi}^{r,m}\right]^{T}_{\tilde{n}\times N}\left[\boldsymbol{\Psi}^{r,m}\right]_{N\times \tilde{n}}\tilde{\mathbf{q}}_{\tilde{n}\times 1} = \left[\boldsymbol{\Psi}^{r,m}\right]^{T}_{\tilde{n}\times N}\bar{\mathbf{u}}^{m}_{\mathbf{N}\times 1} - \left[\boldsymbol{\Psi}^{r,m}\right]^{T}_{\tilde{n}\times N}\left[\boldsymbol{\Phi}^{r,m}\right]_{N\times n}\mathbf{q}_{n\times 1} \tag{13}$$

Thus, we have

$$\tilde{\mathbf{q}}_{\tilde{n}\times 1} = \left[\boldsymbol{\Psi}^{r,m}\right]^{\uparrow}_{\tilde{n}\times N}\bar{\mathbf{u}}^{m}_{N\times 1} - \left[\boldsymbol{\Psi}^{r,m}\right]^{\uparrow}_{\tilde{n}\times N}\left[\boldsymbol{\Phi}^{r,m}\right]_{N\times n}\mathbf{q}_{n\times 1} \tag{14}$$

Substituting the relation given in Eq. (7) into Eq. (14) ends up with

$$\tilde{\mathbf{q}}_{\tilde{n}\times 1} = \left[\boldsymbol{\Psi}^{r,m}\right]^{\uparrow}_{\tilde{n}\times N}\left(\left[\mathbf{I}\right] - \left[\boldsymbol{\Phi}^{r,m}\right]_{N\times n}\left[\boldsymbol{\Phi}^{r,m}\right]^{\uparrow}_{n\times N}\right)\bar{\mathbf{u}}^{m}_{N\times 1} \tag{15}$$

Then, finally one can compute the unmeasured part $\bar{\mathbf{u}}^{u}$ using

$$\bar{\mathbf{u}}^{u}_{\tilde{\mathbf{N}}\times 1} = \left[\boldsymbol{\Phi}^{r,u}\right]_{\tilde{N}\times n}\mathbf{q}_{n\times 1} + \left[\boldsymbol{\Psi}^{r,u}\right]_{\tilde{N}\times \tilde{n}}\left[\boldsymbol{\Psi}^{r,m}\right]^{\uparrow}_{\tilde{n}\times N}\left(\left[\mathbf{I}\right] - \left[\boldsymbol{\Phi}^{r,m}\right]_{N\times n}\left[\boldsymbol{\Phi}^{r,m}\right]^{\uparrow}_{n\times N}\right)\bar{\mathbf{u}}^{m}_{N\times 1} \tag{16}$$

3. Block-wise Modal Expansion Method (BMEM) using GA

3.1 Sensor placement optimization

The sensor placement optimization problem for the vibration pattern reproduction is formulated as follows: Find $\mathbf{X} = \left\{\mathbf{x}^{s}_{1}, \mathbf{x}^{s}_{2}, \cdots, \mathbf{x}^{s}_{N}\right\}^{T}$ such that

$$\underset{\mathbf{X}}{\text{Minimize}} \quad F(\mathbf{X}) \tag{17}$$

$$\text{Subject to:} \quad \left[\mathbf{K} - \omega^{2}\mathbf{M}\right]\boldsymbol{\Phi} = 0 \tag{18}$$

$$\boldsymbol{\Phi}^{r}_{I} = \boldsymbol{\Phi}_{I}\big|_{\mathbf{X}^{s}}, \quad I = 1, 2, \cdots, N \tag{19}$$

Where, $\mathbf{X} = \left\{\mathbf{x}^{s}_{1}, \mathbf{x}^{s}_{2}, \cdots, \mathbf{x}^{s}_{N}\right\}^{T}$ and $F(\mathbf{X})$ indicate the design variable vector containing N sensor positions and the objective function defined in Eq. (3), respectively. Here, Eq. (18) stands for the finite element modal analysis to calculate the original natural modes $\boldsymbol{\Phi}^{org}_{I}$ using a finite element mesh, while Eq. (19) represents the extraction process to construct the reduced numerical

modes $\mathbf{\Phi}_I^r$ corresponding to the sensor positions. A prominent feature of the sensor placement optimization is that the design variable vector $\mathbf{X}$ is not continuous but discrete, which in turn leads to the discontinuity in the objective function $F(\mathbf{X})$. Thus, the mathematical sensitivity can not be defined by the gradient of objective function to the design variable vector (Cho *et al*. 2012). In order to resolve this difficulty in the current discrete-type optimization problem, the mathematical sensitivity-driven search for the direction vector is replaced with the genetic evolution.

The first step in the sensor placement optimization using GA is the generation of an initial population $\wp_G^0 = \left\{ g_{ID}^0 : ID = 1,2,...,N_{pop} \right\}$ consisted of the total of N_{pop} genomes. Where, each genome g_{ID}^0 corresponds to the design variable vector $\mathbf{X} = \left\{ \mathbf{x}_1^s, \mathbf{x}_2^s, \cdots, \mathbf{x}_N^s \right\}^T$ composed of N sensor positions. For the current sensor placement optimization, each genome g_{ID} is expressed by the total number of $m_{TOT} \in \Re^+$ binary bits, where m_{TOT} is calculated according to

$$m_{TOT} = m_1 + m_2 + \cdots m_j + \cdots + m_N \tag{20}$$

by summing the bit numbers $m_j \in \Re^+ (j = 1,2,\cdots,N)$ required for the binary representation of each sensor position vector $\boldsymbol{x}_j^s$. Here, each bit number m_j is determined using the relation of $2^{m_j} \geq N_j^{loc}$, in which N_j^{loc} denotes the total number of possible locations where the *j*-th sensor can be positioned. Then, the genome g_{ID} corresponding to the *ID*-th discrete-type sensor placement $\mathbf{X}_{ID}$ becomes to be coded in the binary form given by

$$g_{ID} = b_1^1 b_1^2 \cdot b_1^{m_1} \cdots \underline{b_j^1 \cdots b_j^{m_j}} \cdots b_N^1 \cdots b_N^{m_N}, \quad ID = 1,2,...,N_{pop} \tag{21}$$

where $b_j^{m_j}$ are either 1 or 0. Here, $\underline{b_j^1 .. b_j^{m_j}}$ stands for the binary string for the *j*-th sensor position $\boldsymbol{x}_j^s$. On the other hand, the decoding to transform each genome g_{ID} in a binary string to the corresponding discrete-type sensor placement $\mathbf{X}_{ID} = \left\{ \mathbf{x}_1^s, \mathbf{x}_2^s, \cdots, \mathbf{x}_N^s \right\}^T$ is carried out string-interval-wise. For example, once a string interval $\underline{b_j^1 .. b_j^{m_j}}$ is decoded into a decimal number according to the binary-decimal converting algorithm, then this decimal number indicates the specific location $\mathbf{x}_j^s$ of the j-th sensor. As will be demonstrated in Section 4.1, this decimal number (i.e., the integer) indicates the node number in the finite element mesh because the sensor positions are to be sought from the possible finite element nodes in the current study.

The initial population $\wp_G^0$ of genomes is generated randomly and a best genome having the highest fitness is to be selected through the iterative genetic evolution. The selection process is made based on the fitness test of genomes in the population, and it prepares the parent genomes to reproduce the offspring genomes through the crossover and mutation operations. In the current study, the roulette-wheel selection method is chosen among several methods introduced so far, and the one-point crossover operator and the classical mutation operator (Michalewicz 2013) are

employed to enlarge the search space of genomes. The fitness of each genome g_{ID}^{k} at the k-th genetic evolution stage is evaluated by

$$U\left(g_{ID}^{k}\right)=1/F\left(g_{ID}^{K}\right) \tag{22}$$

As a stop criterion to terminate the iterative genetic evolution, we use the relative change $\Delta U^{k}=\left|U_{max}^{k+1}-U_{max}^{k}\right|/U_{max}^{k}$ in the maximum fitness value $U_{max}^{k}=\underset{ID}{max}\ U\left(g_{ID}^{k}\right)$ among all the genomes in the population.

The GA-based sensor placement optimization starts with an initial design variable $\boldsymbol{X}^{s,0}$, together with an initial population $\wp_{G}^{0}$, and the setting of crossover and mutation ratios. The genetic evolution is terminated if the relative change ΔU^{k} satisfies the stop criterion (i.e., $\Delta U^{k}\le\varepsilon_{T}$), otherwise the genetic evolution goes to the next iteration. The reader may refer to our previous papers (Jung *et al*. 2015) for more details on the numerical implementation of GA-based sensor placement optimization and the comparison with other methods using different-type objective functions.

*3.2 Block-wise modal expansion method (*BMEM*)*

The above-mentioned basic MEM can effectively provide the overall vibration patterns of structure using a number of known natural modes and the vibration responses measured at several positions, without the information of excitation force. However, the quality of reproduced vibration patterns is influenced by the number of selected modes and measurement points. Furthermore, the selection of natural modes and sensor positions does also influence the quality of vibration pattern reproduction. To overcome the demerit of basic MEM, the residual modal expansion method (RMEM) was introduced by accounting for the effect of high-order modes which were discarded from the mode selection. However, the RMEM provides better vibration pattern reproduction than the basic MEM only when the total number N of sensor positions is not the same with the total number n of selected modes. It is because the vibration patterns reproduced by the RMEM become identical with those obtained by the basic MEM when such two numbers N and n are the same.

In order to explain this feature of the RMEM, let us consider the following term given by

$$\left[\mathbf{I}\right]-\left[\boldsymbol{\Phi}^{r,m}\right]_{N\times n}\left[\boldsymbol{\Phi}^{r,m}\right]_{n\times N}^{\uparrow} \tag{23}$$

which is included in Eq. (15). The matrix $\left[\boldsymbol{\Phi}^{r,m}\right]$ of reduced natural modes becomes a square matrix when N and n are the same, which leads to

$$\left[\boldsymbol{\Phi}^{r,m}\right]^{\uparrow}=\left(\left[\boldsymbol{\Phi}^{r,m}\right]^{T}\left[\boldsymbol{\Phi}^{r,m}\right]\right)^{-1}\left[\boldsymbol{\Phi}^{r,m}\right]^{T}=\left[\boldsymbol{\Phi}^{r,m}\right]^{-1} \tag{24}$$

Hence, the modal participation factors $\tilde{\mathbf{q}}_{\tilde{n}\times 1}$ of the discarded higher-order modes completely vanish, and which results in $\bar{\mathbf{u}}_{\tilde{N}\times 1}^{u}\left(\mathbf{x};t\right)=\mathbf{0}$. The condition for the RMEM that N should not be the same with n becomes a crucial obstacle for improving the quality of vibration pattern

reproduction, because the more the modes are selected the more the measured responses are required.

The disadvantages of the basic MEM and RMEM could be successfully overcome by the BMEM which is introduced in this paper. Referring to Fig. 3, a whole frequency range of interest is divided into the total of k overlapped blocks, where the frequency bands $\Delta\omega_I$ of each block are non-uniformly determined such that

$$\Delta\omega_I = \omega_I^L \sim \omega_I^R, \quad I = 1,2,\cdots,k \tag{25}$$

based on the natural modes selected for the vibration pattern reproduction for each block. And, the whole vibration field of structure is expressed by the sum of block-wise vibration fields as follows

$$\mathbf{u}(\mathbf{x};\omega) = \mathbf{u}^1(\mathbf{x};\omega) + \mathbf{u}^2(\mathbf{x};\omega) + \cdots + \mathbf{u}^k(\mathbf{x};\omega) \tag{26}$$

where the frequency ranges of each block-wise vibration field are restricted within the corresponding frequency bands. And, each vibration field $\mathbf{u}^I(\mathbf{x};\omega)$ is reproduced by the basic MEM such that

$$\mathbf{u}^I_{N\times 1} = \left[\boldsymbol{\Phi}^{I,r}\right]_{N\times n}\mathbf{q}^I_{n\times 1}, \quad I = 1, 2, \cdots, k \tag{27}$$

Here, $\left[\boldsymbol{\Phi}^{I,r}\right]$ and $\mathbf{q}^I$ are the block-wise reduced natural modes and the modal participation factors.

In the BMEM, the vibration responses $\bar{\mathbf{u}}_{\mathbf{N}\times 1}$ at all the sensor positions are measured once and used to determine the modal participation factors $\mathbf{q}^I$ for all the frequency blocks according to

$$\mathbf{q}^I_{n\times 1} = \left[\boldsymbol{\Phi}^{I,r}\right]^{\uparrow}_{n\times N}\bar{\mathbf{u}}^I{}_{N\times 1}, \quad I = 1, 2, \cdots, k \tag{28}$$

Where, $\bar{\mathbf{u}}^I_{N\times 1} = \bar{\mathbf{u}}_{\mathbf{N}\times 1}\big|_{Block\ I}$ indicates the measured vibration response restricted to the I-th frequency block. In the current study, the total numbers of sensor positions and the selected modes are set equally (i.e., $N = n$). And the total number of selected modes is set equally for all the frequency blocks and the frequency blocks are not uniform. The natural modes are selected from the original natural modes in sequence, so that frequency bands of each frequency block are determined by the lowest and highest modes selected for each frequency band, as shown in Fig. 3.

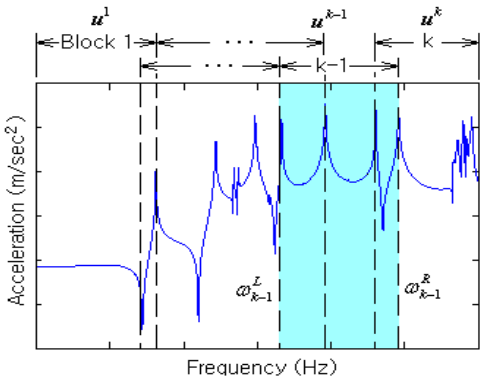

Fig. 3 Schematic representation of the BMEM

4. Numerical experiments

The proposed block-wise modal expansion method incorporated with the GA-based sensor placement optimization is implemented and compared with two conventional MEMs, ABAQUS and MSC/Nastran. For the sake of more reliable verification of the current BMEM, two commercial softwares are taken. For this purpose, we consider a hollow cylindrical shell-like structure shown in Fig. 4(a) of the thickness $t = 0.008m$, which is manufactured with steel having the Young's modulus E of $200GPa$, Poisson's ratio ν of 0.3 and ρ of $7{,}850kg/cm^3$. Both ends of the cylinder are closed by discs and a thick rectangular stiffener of the thickness $t = 0.01m$ is built within the cylinder. Cartesian co-ordinate system is positioned at the center of the right disc, and the vertical excitation forces F_1 and F_2 are applied to the internal rectangular stiffner. The whole structure is uniformly discretized with 4-node shell elements and the total number of elements reaches 11,328.

The total of 64 vibration sensors are used to measure the nodal vibration responses, and those are to be positioned on the outer surface of cylindrical shell structure. The outer surface is uniformly discretized by 80×80 in the horizontal and circumferenctial directions. The total number N_j^{loc} of possible locations where the *j*-th sensor can be positioned is identical with the total number of finite element nodes on the outer surface, except for the nodes lying on the outer surface-disc interfaces. In case of the current 80×80 uniform mesh for the outer surface, the total number N_j^{loc} becomes $79 \times 80 = 6{,}320$. Then, from the relation of $2^{m_j} \geq N_j^{loc}$, the total of 13 binary bits are required to represent each sensor position, and each genome g_{ID} representing the placement $\boldsymbol{X}_{ID} = \left\{ \boldsymbol{x}_1^s, \boldsymbol{x}_2^s, \cdots, \boldsymbol{x}_{64}^s \right\}^T$ of 64 sensors is expressed by the total of 832 binary bits.

The population size N_{pop} is set by 50 while the crossover and mutation ratios are chosen by 0.6 and 0.03 respectively, as is conventionally taken. The finite element modal analyses of the structure were performed by MSC/Nastran, a commercial FEM code, to compute the original natural modes $\boldsymbol{\Phi}_I^{org}$, from which the total of 64 reduced numerical modes $\boldsymbol{\Phi}_I^r$ were constructed according to Eq. (1). The reduced modes were selected by choosing the lowest 64 natural modes within the frequency range of $0 \sim 390Hz$ from the original natural modes which were directly obtained by MSC/Nastran. The iteration histories of the fitness values without applying the stop criterion are represented in Fig. 5(a), where it is clearly observed that both the maximum fitness value and the mean fitness value converge uniformly and stably with the number of generations. The optimum placement of 64 sensors is represented in Fig. 4(b), for which the convergence criterion ε_T is set by 0.1 and the genetic evolution terminated in about 2,000 iterations. Fig. 5(b) represents the modal assurance criterion (MAC) of 64 reduced numerical modes $\boldsymbol{\Phi}_I^r$, where the contrast between the diagonal and off-diagonal values is apparent such that all the diagonal values are almost unity while the off-diagonal values are sufficiently small except for few off-diagonal values.

Through the parametric experiments to the number of sensors, it was observed that the probability of error in finding the optimum sensor placement decreases in proportional to the number of sensor. It is because the possibility of GA to converge a local minimum deceases as the number of sensors increases. This observation is consistent with the result given in a paper by

Worden and Burrows (2001), where the influence of the number of sensors on the optimal sensor placement is presented. It was also observed that the quality of reproduced vibration pattern becomes improved in proportional to the number of sensors, because the orthogonality between the reduced numerical modes becomes better and therefore the accuracy of calculated modal participation factors becomes higher.

Next, for the vibration pattern reproduction, the frequency range of interest is set by $0 \sim 400 Hz$ and the selected 64 reduced numerical modes $\mathbf{\Phi}_I^r$ are taken. First, the vibration pattern reproduction was made by the basic MEM, and the results are compared with those that were obtained by the direct forced vibration analysis using ABAQUS with the same FEM mesh and two external excitations shown in Fig. 4. Meanwhile, the noise included in measurements deteriorates the quality of vibration pattern reproduction because it affects the reliability of sensor placement and modal participation factors that were determined using the measured vibration data. For the current study, the phase reference measurement (Cho and Kang 2016), together with the averaging of measured vibration data, was employed to suppress the influence of noise. In this measurement technique, the acceleration response at any response point is calculated using the phase reference spectrum of response point which is calculated from the relative phase difference between the response point and the reference basis point. The reader may refer to Cho and Kang (2016) for more detailed explanation.

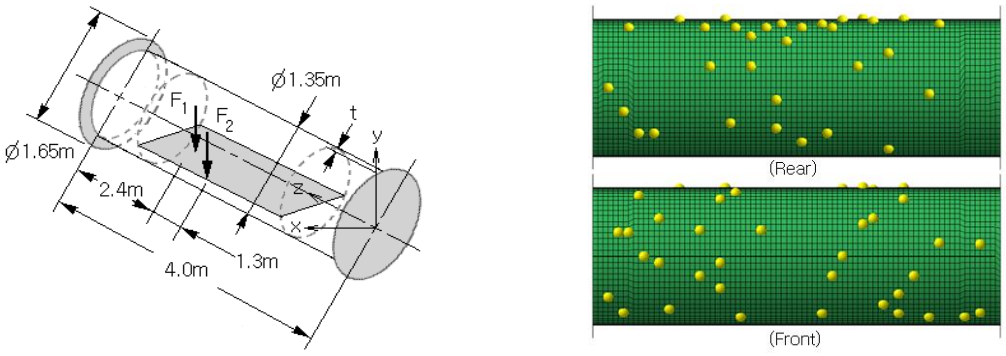

(a) (b)

Fig. 4 (a) A hollow cylindrical shell structure and (b) optimum sensor placement

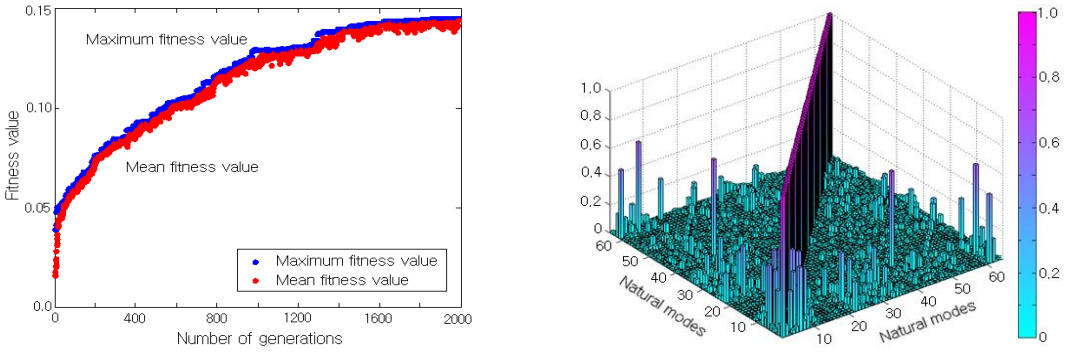

(a) (b)

Fig. 5 Optimization results obtained by GA: (a) iteration histories of fitness value and (b) MAC

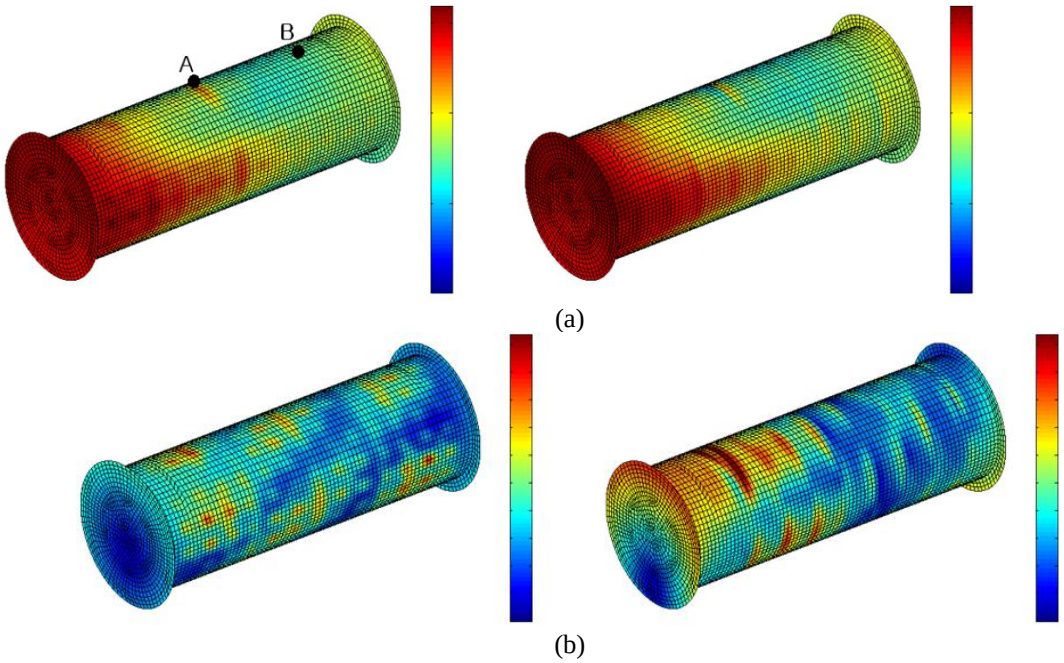

Fig. 6 Comparison of the vibration patterns between ABAQUS (left) and basic MEM (right): (a) at $60Hz$ and (b) at $180Hz$

Fig. 6 compares the vibration patterns at two different frequencies between the basic MEM and ABAQUS. The quantity in all the figures showing the vibration patterns in this paper indicates the absolute displacement. The patch function of MatLab is employed to construct the color contour maps, and the displacement magnitude is adjusted by the jet color scale. It is clearly observed that the basic MEM provides the vibration pattern which is consistent well with ABAQUS at $60Hz$. But, one can see the quite difference in the vibration patterns at $180Hz$ between ABAQUS and the basic MEM. It can be inferred from this comparison that the basic MEM can provide the reliable vibration pattern at low frequency but its accuracy becomes lower as the frequency of interest increases. This fact can be also confirmed from the comparison of the nodal frequency responses shown in Fig. 7, where the positions of two nodes A and B on the shell outer surface are indicated in Fig. 6(a). The basic MEM shows the nodal frequency responses consistent with ABAQUS up to $225Hz$ at node A and up to $170Hz$ at node B, but it shows a remarkable deviation from ABAQUS at the frequencies higher than such frequency levels. Therefore, the applicability of basic MEM is limited to only the lower frequency range.

Next, the residual modal expansion method (RMEM) was implemented for which 50 higher-order discarded modes as well as the lowest 50 selected modes are taken for the vibration pattern reproduction. In other words, the total of 100 reduced modes are used for the total of 64 points of measurement, which satisfies the condition imposed on the RMEM that the number of measurement points should not be the same with the number of selected modes. In Figs. 8 and 9, the vibration patterns reproduced by the RMEM at 200 and $400Hz$ are compared with MSC/Nastran and the basic MEM. Differing from the basic MEM, it is observed from Fig. 8 that

the RMEM provides the vibration pattern which is in a good agreement with MSC/Nastran at $200\,Hz$.

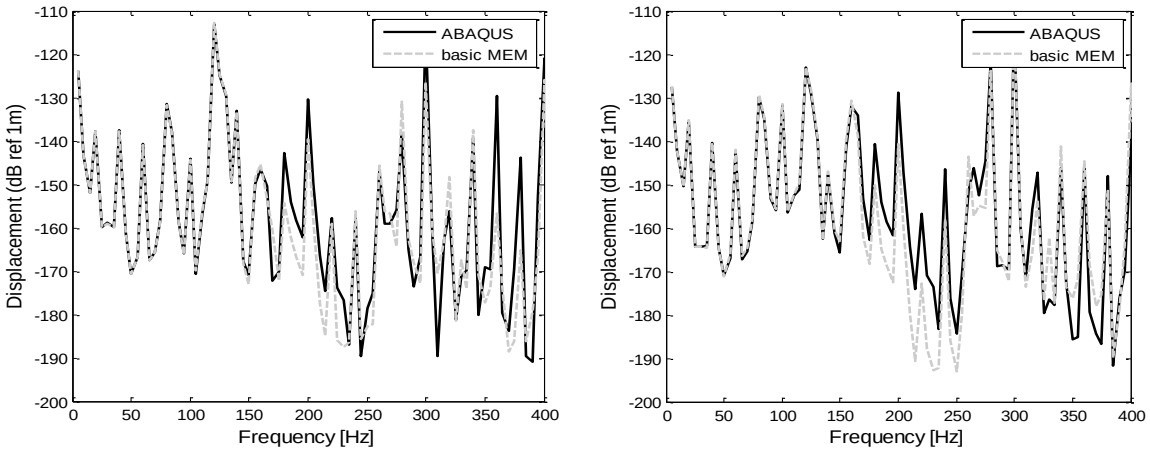

(a) (b)

Fig. 7 Comparison of the frequency responses of nodal Y-displacement for the basic MEM: (a) at node A and (b) at node B

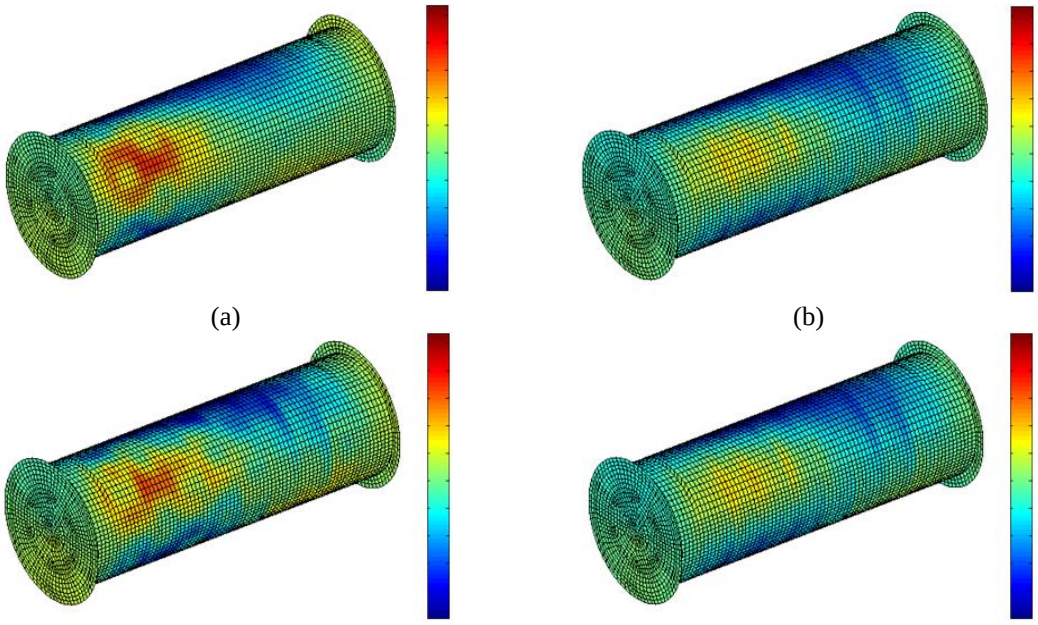

(a) (b)

(c) (d)

Fig. 8 The vibration patterns at $200\,Hz$: (a) Nastran, (b) basic MEM, (c) RMEM and (d) BMEM

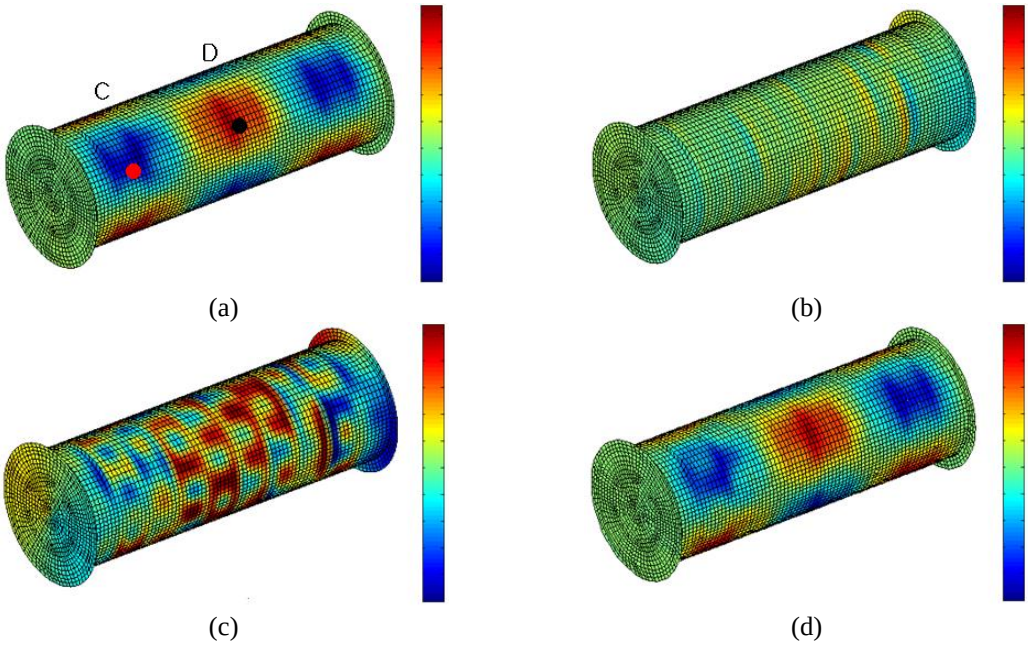

Fig. 9 The vibration patterns at $400\,Hz$: (a) Nastran, (b) basic MEM, (c) RMEM and (d) BMEM.

But, it shows the significant discrepancy at $400\,Hz$ like the basic MEM. Fig. 10 comparatively represents the frequency responses of nodal accelerations within the frequency range of $0 \sim 600\,Hz$ at two different nodes C and D indicated in Fig. 9(a). Where, it is observed that the RMEM shows an agreement with MSC/Nastran to some extent in the lower frequency range like the basic MEM, but in the higher frequency range it shows the remarkable discrepancy from MSC/Nastran. What is worse, the RMEM leads to the frequency responses that are worse than the basic MEM at certain frequencies. Thus, it is confirmed that the RMEM can not provide the reliable vibration patterns at high frequencies, too.

At the final step, the block-wise modal expansion method (BMEM) is implemented, for which the frequency range for determining the modal participation factors $\mathbf{q}$ is set by $0 \sim 600\,Hz$ and it is divided into three blocks as follows:

- Block 1) $\Delta\omega_1 = 0 \sim 390\,Hz$, Number of selected modes & measurements: $n^1 = N = 64$
- Block 2) $\Delta\omega_2 = 276 \sim 492\,Hz$, Number of selected modes & measurements: $n^2 = N = 64$
- Block 3) $\Delta\omega_3 = 391 \sim 592\,Hz$, Number of selected modes & measurements: $n^3 = N = 64$

Among the original natural modes obtained by MSC/Nastran, the lowest 64 modes are selected for block 1 and the next 64 modes (i.e., from the 65-th mode to the 128-th mode) for block 3. Meanwhile, the intermediate 64 modes starting from the 33-th mode to the 96-th mode are taken for block 2. The frequency bands of three blocks were determined by the frequency levels of the lowest and highest modes within each block, as mentioned earlier.

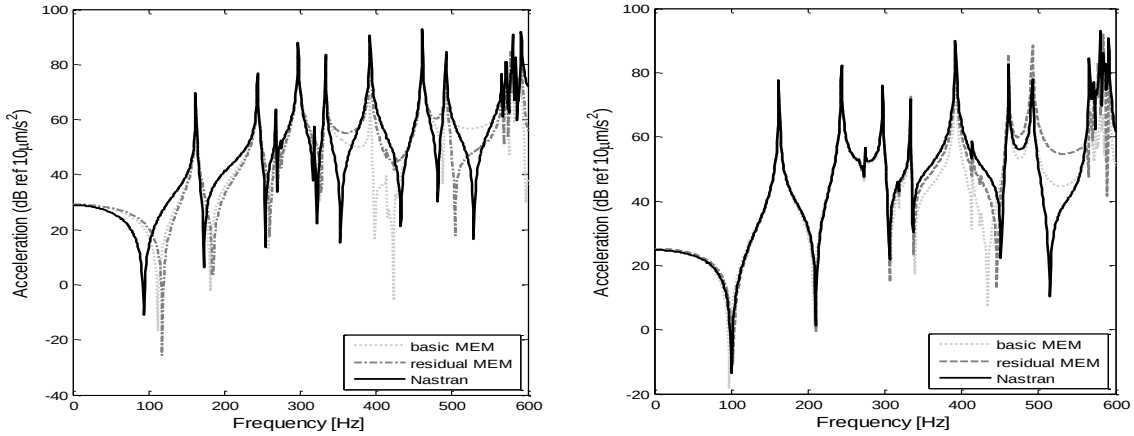

Fig. 10 Comparison of the frequency responses of nodal acceleration for RMEM: (a) at node C and (b) at node D

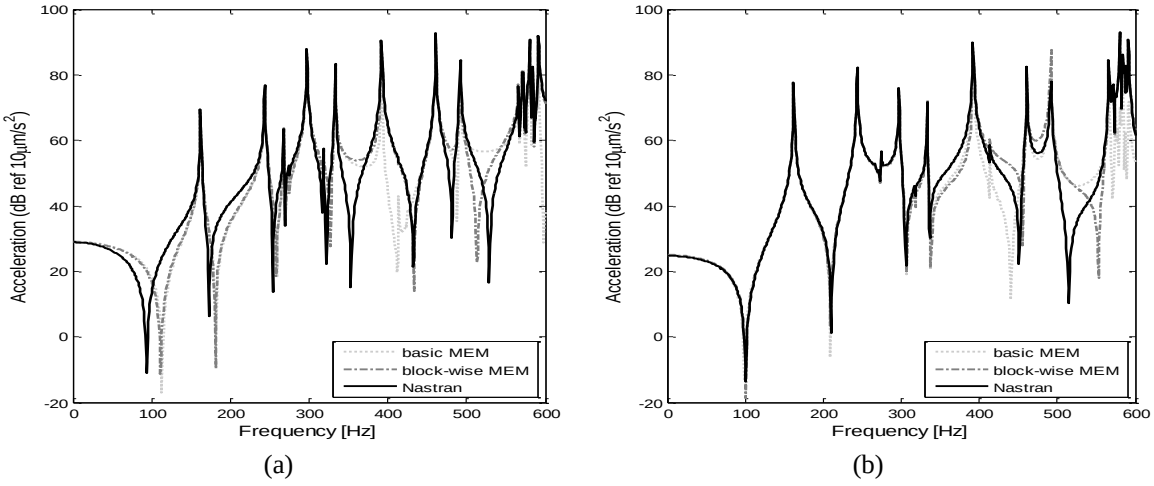

Fig. 11 Comparison of the frequency responses of nodal acceleration for BMEM: (a) at node C and (b) at node D

The vibration patterns reproduced by the BMEM are compared with MSC/Nastran and the other two MEMs in Figs. 8 and 9. It is observed from Fig. 8 that the BMEM shows the result similar to the basic MEM and RMEM at $200Hz$. But, from Fig. 9, one can clearly see that it provides the vibration pattern which is in an excellent agreement with MSC/Nastran at $400Hz$. It can be also confirmed from the frequency responses of nodal accelerations shown in Fig. 11 at two different nodes. The basic MEM provides the frequency response similar to MSC/Nastran up to $400Hz$, but it shows the remarkable discrepancy at the frequencies higher than $400Hz$. On the other hand, the BMEM leads to the frequency response that is generally similar to MSC/Nastran

over a whole frequency range. Thus, it has been justified that the BMEM can provide the remarkably improved vibration field better than the basic and RMEM, particularly at high frequencies.

5. Conclusions

A new modal expansion method for reproducing the vibration patterns of elastic structures, called the block-wise modal expansion method (BMEM) incorporated with the GA-based sensor placement optimization, has been introduced in this paper. In order to overcome the quality deterioration of reproduced vibration patterns at high frequencies of the conventional basic and residual modal expansion methods, the vibration patterns in the BMEM are reproduced by superposing the block-wisely reproduced vibration patterns. A whole frequency range of interest is divided into several overlapped frequency blocks and the vibration field reproduction is made by block by block with different natural modes and different modal participation factors. Meanwhile, the sensor positions which greatly influence the quality of vibration field reproduction were determined by the discrete-type optimization making use of GA and the modal assurance criterion (MAC).

Through the numerical experiment with a hollow cylindrical shell-like structure for the vibration pattern reproduction, the following main observations are drawn.

- The vibration pattern and the frequency response that were reproduced by the basic MEM are consistent well with ABAQUS only at the remarkably low frequency range up to 60~170 Hz.
- In case of the residual MEM (RMEM), the numerical accuracy becomes improved slightly when compared with the basic MEM. But, its improvement is observed to be limited up to 200 Hz from the comparison with MSC/Nastran, what is worse, it provides the frequency response worse than the basic MEM at certain frequencies.
- On the other hand, the present BMEM provides the significantly improved vibration field better than the basic MEM and RMEM, particularly at high frequencies.

Acknowledgements

This work was partially supported by the Hongik University new faculty research support fund.

References

Allaei, D. and Soedel, W. (1986), "Natural frequencies and modes of rings that deviate from perfect axisymmetry", *J. Sound Vib.*, **111**(1), 9-27.

Allemang, R.J. and Brown, D.L. (1982), "A correlation coefficients for modal vector analysis", *Proceedings of International Modal Analysis Conference.*

Bernard, M.L. and Bronowicki, A.J. (1994), "Modal expansion method for eigensensitivity with repeated roots", *AIAA J.*, **32**, 1500-1506.

Brehm, M., Zabel, V. and Bucher, C. (2010), "An automatic mode pairing strategy using an enhanced modal assurance criterion based on modal strain energies", *J. Sound Vib.*, **329**, 5375-5392.

Carden, E.P. and Fanning, P. (2004), "Vibration based condition monitoring: A review", *Struct. Health*

Monit., **3**(4), 355-377.
Chen, H.P. (2010), "Mode shape expansion using perturbed force approach", *J. Sound Vib*., **329**, 1177-1190.
Cho, J.R. and Lee, J.K. (2001), "Finite element techniques for the free-vibration and seismic analysis of liquid-storage tanks", *Finite Elem. Anal. Des*., **6-7**, 467-483.
Cho, J.R., Lee, J.H., Jeong, K.M. and Kim, K.W. (2012), "Optimum design of run-flat tire insert rubber by genetic algorithm", *Finite Elem. Anal. Des*., **52**, 60-70.
Cho, Y.U. and Kang, G.H. (2016), "The force identification of 200kW IPMSM using phase reference spectrum", *Proceedings of the 2016 IEEE Transportation Electrification Conference and Expo, Asia-Pacific (ITEC)*, Busan, Korea.
Friswell, M.I. and Mottershead, J.E. (1995), *Finite Element Modal Updating in Structural Dynamics*, Kluwer Academic Publishers, Netherlands.
Han, J.H. and Lee, I. (1999), "Optimal placement of piezoelectric sensors and actuators for vibration control of a composite plate using genetic algorithms", *Smart Mater. Struct*., **8**(2), 257-268.
Hiramoto, K., Doki, H. and Obinata, G. (2000), "Optimal sensor/actuator placement for active vibration control using explicit solution of algebraic Riccati equation", *J. Sound Vib*., **229**(5), 1057-1075.
Jiménez, F.J. and De Frutos, J. (2005), "Virtual instrument for measurement, processing data, and visualization of vibration patterns of piezoelectric devices", *Computer Standards & Interfaces*, **27**, 653-663.
Jung, B.K., Cho, J.R. and Jeong, W.B. (2015), "Sensor placement optimization for structural modal identification of flexible structures using genetic algorithm", *J. Mech. Sci. Technol*., **29**(7), 2775-2783.
Larson, C.B., Zimmerman, D.C. and Marek, E.L. (1994), "A comparison of modal test planning techniques: Excitation and sensor placement using the NASA 8-bay truss", *Proceedings of the 12th International Modal Analysis Conference.*
Li, F.L., Hu, X.Y. and Zhang, L. (2013), "Left and right inverse eigenpairs problem for κ-Hermitian matrices", *J. Appl. Math*., ID 230408, 1-6.
Lin, J. and Parker, R.G. (1999), "Sensitivity of planetary gear natural frequencies and vibration modes to model parameters", *J. Sound Vib*., **228**(1), 109-128.
McConnell, K.G. (1995), *Vibration Testing - Theory and Practice*, John Wiley & Sons, Singapore.
Michalewicz, Z. (2013), *Genetic Algorithms+Data Structures=Evolution Programs*, Springer-Verlag, New York.
Papadimitriou, C. (2004), "Optimal sensor placement methodology for parametric identification of structural systems", *J. Sound Vib*., **278**, 923-947.
Poston, W.L. and Tolson, R.H. (1992), "Maximizing the determinant of the information matrix with the effective independence method", *J. Guid. Control Dynam*., **15**(6), 1513-1514.
Sas, P., Bao, C., Augusztinovicz, F. and Desmet, W. (1995), "Active control of sound transmission through a double panel partition", *J. Sound Vib*., **180**(40), 609-625.
Stephan, C. (2012), "Sensor placement for modal identification", *Mech. Syst. Signal Pr*., **27**, 461-470.
Worden, K. and Burrows, A.P. (2001), "Optimal sensor placement for fault detection", *Eng. Struct.*, **23**, 885-901.
Yi, T.H., Li, H.N. and Gu, L.M. (2012), "Sensor placement for structural health monitoring of Canton Tower", *Smart Struct. Syst.*, **19**(4), 313-329.
Yi, T.H., Li, H.N. and Gu, M. (2011), "Optimal sensor placement for structural health monitoring based on multiple optimization strategies", *Struct. Des. Tall Spec*., **20**(7), 881-900.
Yi, T.H., Li, H.N. and Wang, C.W. (2015), "Multiaxial sensor placement optimization in structural health monitoring using distributed wolf algorithm", *Struct. Control Health Monit*., **23**(4), 719-734.
Yi, T.H., Li, H.N. and Wang, X. (2013), "Multi-dimensional sensor placement optimization for Canton Tower focusing on application demands", *Smart Struct. Syst*., **12**(3-4), 235-250.

CY

Nomenclature

$\left[\boldsymbol{\Phi}^{org}\right]$	original natural modes
$\left[\boldsymbol{\Phi}\right]_{m\times n}$	selected natural modes $\left(=\left[\boldsymbol{\Phi}\right]\right)$
$\left[\boldsymbol{\Phi}^{r}\right]_{N\times n}$	reduced numerical natural modes $\left(=\left[\boldsymbol{\Phi}^{r}\right]\right)$
MAC_{IJ}	modal assurance criterion $\left(=MAC\left(\left\{\boldsymbol{\Phi}_I\right\}\left\{\boldsymbol{\Phi}_J\right\}\right)\right)$
$F(\mathbf{X})$	objective function
$\mathbf{X}$	design variable vector $\left\{\mathbf{x}_1^s, \mathbf{x}_2^s, \cdots, \mathbf{x}_N^s\right\}^T$
$\bar{\mathbf{u}}(\mathbf{x};t)$	nodal displacement vector
$\mathbf{q}(t)$	vector of modal participation factors
$\left[\mathbf{M}\right]$	mass matrix
$\left[\mathbf{C}\right]$	damping matrix
$\mathbf{F}$	load vector
Q_I	normalized forces $\left(=\left\{\boldsymbol{\Phi}_I\right\}^T\mathbf{F}\right)$
q_I	modal participation factors
ς	damping ratio
$\left[\boldsymbol{\Phi}^{r}\right]^{\uparrow}$	left generalized inverse matrix of $\left[\boldsymbol{\Phi}^{r}\right]$
$\left[\boldsymbol{\Psi}\right]$	discarded higher-order natural modes
$\bar{\mathbf{u}}_{N\times 1}^{m}(\mathbf{x};t)$	measured nodal displacement
$\bar{\mathbf{u}}_{\tilde{N}\times 1}^{u}(\mathbf{x};t)$	unmeasured nodal displacement
$\tilde{\mathbf{q}}_{\tilde{n}\times 1}$	modal participation factors of unselected natural modes
g_{ID}	*ID*-th genome
$\wp_G^0$	initial population
N_{pop}	population size
N_i^{case}	case number of the *i*-th position vector $\mathbf{x}_I^s$
$\mathbf{X}_{ID}$	*ID*-th discrete-type sensor placement
b_i	binary bits
$U\left(g_{ID}^k\right)$	fitness of *ID*-th genome
ε_T	tolerance of stop criterion
Δf_I	frequency band of *I*-th block
$\mathbf{u}^I(\mathbf{x};\omega)$	block-wise vibration fields
$\left[\boldsymbol{\Phi}^{I,r}\right]$	block-wise reduced natural modes
$\mathbf{q}^I$	block-wise modal participation factors